

# Multi-scale Stress Analysis and 3D Fitting Structure of Superconducting Coils for the Helical Fusion Reactor

Hitoshi Tamura (田村 仁), Nagato Yanagi (柳 長門), Kazuya Takahata (高畑 一也), Akio Sagara (相良 明男), Satoshi Ito (伊藤 悟), and Hidetoshi Hashizume (橋爪 秀利)

**Abstract**—Conceptual design studies for the LHD-type helical reactor, FFHR-d1, are being conducted in the National Institute for Fusion Science. Three different cooling schemes and conductor type have been proposed for the superconducting magnet system. A multi-scale structural analysis is used to assess the mechanical characteristics of the magnet structure taking into account the types of cooling schemes and superconductors. Multi-scale analysis evaluates both the stress distribution in the coil support structure and local stress in the constituents of the superconductors without rebuilding a finite element model of the support structure. Concerning a segmented fabrication of the helical coils using a high temperature superconductor, feasibility of segment installation is confirmed using 3D printing model, which identifies the maximum segment length and the necessary gap in the coil casing to install a segment.

**Index Terms**— Additive manufacturing, Fusion reactor design, helical fusion reactor, multi-scale analysis, superconducting magnets.

## I. INTRODUCTION

THE LARGE HELICAL DEVICE (LHD)-TYPE helical fusion reactor is well suited to be used as a fusion power plant because it has attractive features such as steady-state operation in the absence of a plasma current drive. The National Institute for Fusion Science (NIFS) is developing a conceptual design of the LHD-type helical reactor, FFHR-d1 [1], [2]. Research and development of reactor components are being conducted in collaboration with Japanese universities. The superconducting magnet system of the FFHR-d1 includes one pair of helical coils (HCs) and two pairs of vertical field coils (VFCs). The HCs have major and minor radii of 15.6 m and 3.744 m, respectively. The magnetomotive force of each HC is 36.66 MA, and the magnetic stored energy reaches 160 GJ. Several cooling schemes have been proposed for the coils, including forced flow with a cable-in-conduit conductor

(CICC) using a low temperature superconductor (LTS) [3], indirect cooling with an LTS [4], [5], and helium gas cooling with a high temperature superconductor (HTS) [6], [7]. Candidates for use as the superconductor are  $\text{Nb}_3\text{Sn}$  and  $\text{Nb}_3\text{Al}$  for the LTS, and  $\text{YBa}_2\text{Cu}_3\text{O}_7$  (YBCO) for the HTS, as the maximum magnetic field will be 11.8 T.

Multi-scale stress analysis has been developed for a structure made of composite material with a heterogeneous microstructure [8]. This method is appropriate for assessing the mechanical behavior of the magnet system under the various candidate cooling schemes and superconductor types because the components of the superconducting cable/tape, superconductor, and coil support structure have scale orders of mm, cm, and greater than 10 m, respectively; the superconductor has an identical cross-section throughout its longitudinal direction.

If an LTS is used, the coil is wound continuously, whereas segmented fabrication is possible for an HTS [6], [7]. This study also investigated the feasibility of winding using a 3D CAD system and additive manufacturing (3D printing).

## II. MULTI-SCALE ANALYSIS OF MAGNET SYSTEM

### A. Homogenization analysis of superconductors

Fig. 1 shows the schematic of the FFHR-d1 and the fundamental design of the helical coil winding section, which consists of 390 turns of the superconductor. Each superconductor has a 62 mm square shape. A single superconductor carries a current of 94 kA. Both the gas-cooled HTS, and the CICC LTS type superconductors, have been designed according to this specification. The indirect-cooled LTS type has a different cross-sectional geometry, since cooling panels are inserted between every one to four layers of winding [4], [5]. We assumed that the superconductor for the indirect-cooled type had the same square cross-section as the others when comparing its rigidity in the coil support structure by maintaining the volume fraction of the internal materials such as the superconducting cable, jacketing components, and insulator. The cross-sections of the three types of superconductor are shown in Fig. 2.

As the first step of the multi-scale analysis, homogenization was applied to the unit cell of the superconductor, which had a periodic symmetry in the three axes of width, height, and length. We set the unit length at 62 mm to give the unit cell a

This work was supported in part by Ministry of Education, Culture, Sports, Science, and Technology (MEXT) Grant-in-Aid for Scientific Research (S), 26220913, 2015, and by the grant from NIFS (No. UFFF031), 2015.

H. Tamura, N. Yanagi, K. Takahata, and A. Sagara are with the National Institute for Fusion Science, Toki 509-5292, Japan (e-mail: tamura@nifs.ac.jp; yanagi@lhd.nifs.ac.jp; takahata@lhd.nifs.ac.jp; sagara@lhd.nifs.ac.jp).

S. Ito and H. Hashizume are with the Department of Quantum Science and Energy Engineering, Graduate School of Engineering, Tohoku University, Sendai 980-8579, Japan (e-mail: satoshi.ito@qse.tohoku.ac.jp; hidetoshi.hashizume@qse.tohoku.ac.jp).

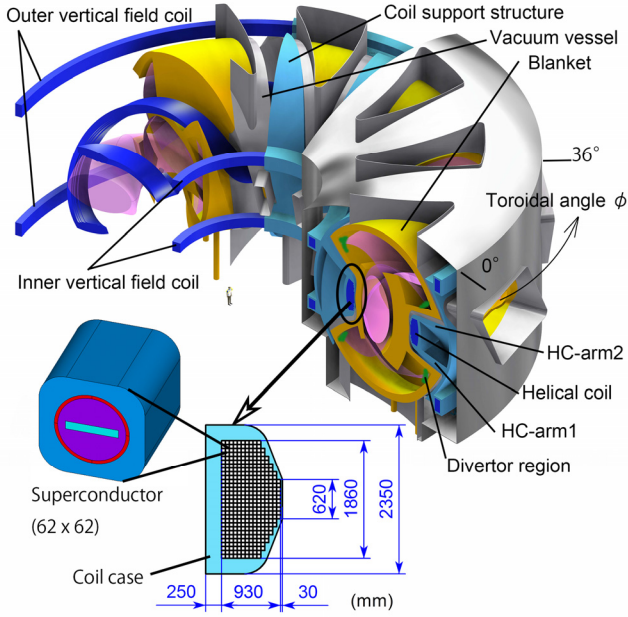


Fig. 1. Schematic of the helical fusion reactor FFHR-d1.

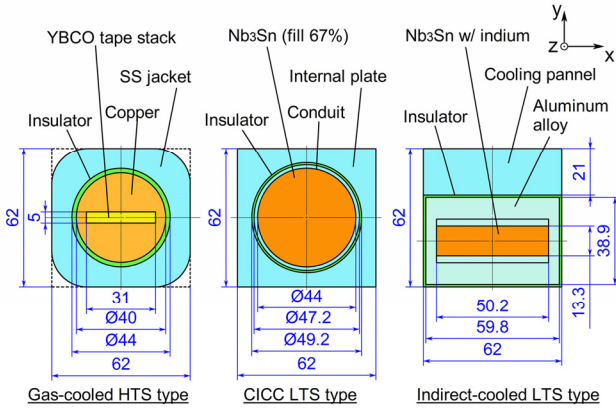


Fig. 2. Cross-section of the superconductors for gas-cooled HTS (left), CICC LTS (center), and indirect-cooled LTS (right). The indirect-cooled HTS type here is different from the candidate design.

cubic structure. A certain unidirectional strain ( $\epsilon_x, \epsilon_y, \epsilon_z, \epsilon_{xy}, \epsilon_{yz}, \epsilon_{xz}$ ) was applied to the unit cell and the stress distribution against each strain was calculated. This allowed the equivalent physical properties of the unit cell to be obtained using the relationship between the strain and the averaged stress. We assumed that the Young's moduli/Poisson's ratios of stainless steel, copper, and aluminum alloy were 200 GPa / 0.3, 120 GPa / 0.3, and 77 GPa / 0.327, respectively [9]–[11]. Those for the Nb<sub>3</sub>Sn regions in the CICC LTS and the indirect LTS were assumed to be 67 GPa / 0.3 and 88 GPa / 0.3, taking account of the void fraction or filling material. The cooling panel comprised a stainless steel plate and a copper panel with a cooling channel [5]. The rigidity of the cooling panel section was assumed to be 90% that of stainless steel. The physical properties of the insulator for the gas-cooled HTS and the CICC LTS were based on those used for the ITER coils [12]. The indirect-cooled LTS type normally has ceramic insulation, with 80 GPa / 0.3. The structural analysis was conducted using

TABLE I  
HOMOGENIZED EQUIVALENT PHYSICAL PROPERTIES OF THE SUPERCONDUCTORS

	Gas-cooled HTS	CICC LTS	Indirect-cooled LTS
$E_x$ (GPa)	79.6	121.3	114.0
$E_y$ (GPa)	79.4	121.3	103.1
$E_z$ (GPa)	156.1	144.9	114.0
$G_{xy}$ (GPa)	44.6	39.8	37.4
$G_{yz}$ (GPa)	43.9	47.7	37.5
$G_{xz}$ (GPa)	44.0	47.7	43.6
$\nu_{xy}$	0.394	0.279	0.314
$\nu_{yz}$	0.149	0.244	0.283
$\nu_{xz}$	0.150	0.244	0.308

$E_i$  is Young's modulus in the  $i$ -direction,  $\nu_{ij}$  is Poisson's ratio for a transverse strain in the  $j$ -direction when stressed in the  $i$ -direction, and  $G_{ij}$  is the shear modulus in the  $i$ - $j$  plane. The local coordinate system is shown in Fig. 2.

ANSYS 16.1.

The equivalent physical properties calculated from the homogenization analysis are shown in Table I. The longitudinal rigidity  $E_z$  was similar to that calculated using the rule of mixtures with an area fraction of the component materials, while the rigidity perpendicular to the longitudinal direction  $E_x, E_y$  appeared to depend not only on properties of the material but also on the outline shape of the superconductor. In the actual conductor, there would be a void, gap, or slip among conductor elements. An experimental evaluation is needed to validate the estimated physical properties before the final design. The equivalent physical properties obtained here were used to describe the properties of the finite elements at the coil winding section in the general assembly (whole structure) model of the coil support structure.

### B. Stress analysis of the coil support structure

The coil support structure of the FFHR-d1 comprises the coil case, arm, and a torus-shaped shell, as shown in Fig. 1. As part of a multipath strategy of the FFHR-d1 [2], an alternative design has been proposed for the coil support structure with the aim of mitigating neutron irradiation of the divertor components [13]. To allow the divertor to be moved to a lower neutron irradiation location, the arms between the coils case and the torus-shaped shell must be partially removed. Since the arms play an important role in strengthening the coil support structure, the stress will be more severe than in the original design. The stress and strain in the superconductor are also assumed to be higher. We analyzed the stress on the coil support structure in the novel divertor design. Since the geometrical position of the HCs and VFCs was unchanged, the electromagnetic force induced by the coils was the same as those in the original design [14]. There is no difference in the coil support structure among the three types of candidate conductors.

Fig. 3 shows the resulting von Mises stress distribution on the deformed shape in the gas-cooled HTS. Both the maximum stress and the amount of deformation appeared at an edge of the removed arms. For the HC, we investigated the axial strain in the longitudinal direction of the superconductor, and in-plane shear stress on the cross-section of the coil, perpendicular to the winding direction. Fig. 4 shows the

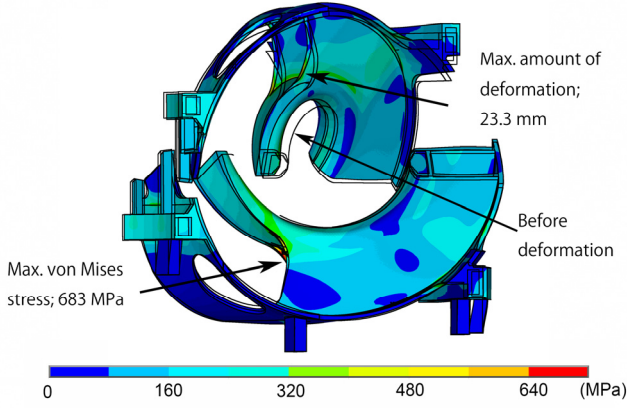


Fig. 3. Results from whole structure analysis. Von Mises stress distribution with deformed image in case of the gas-cooled HTS type is shown. Because of the cyclic symmetry, only a 36° region of the structure was calculated.

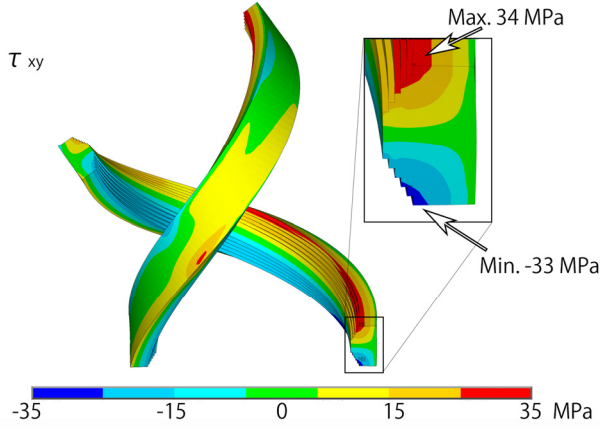


Fig. 4. Distribution of in-plane shear stress in the HCs in case of the gas-cooled HTS type.

distribution of the in-plane shear stress for the HC. The maximum stress appeared near the side of the coil case at a toroidal angle of 0°. The distribution of the stress, strain, and displacement were similar in the three types of superconductor. The maximum value for each case is given in Table II.

The longitudinal rigidity of the superconductor was the dominant factor in the maximum stress and deformation of the coil support structure. The higher the Young's modulus in the longitudinal direction was, the lower the maximum stress, strain, and deformation became. In contrast, the in-plane stress in the HC rose as the shear module corresponding to the plane increased. The stress level of the coil support structure remained within the permissible limit for the stainless steel [15], and the maximum longitudinal strain was acceptable from the viewpoint of the tensile strength of the superconducting materials [11], [16].

### C. Localization analysis of the superconductor

Based on the results of the stress analysis of the coil support structure, we analyzed the internal stress distribution of the superconductor under high HC in-plane stress. Local stress distribution in the superconductor was calculated by applying the strain of an element volume from the whole-structure analysis to the analytical model used in the homogenization

TABLE II  
MAXIMUM VALUE OBTAINED FROM THE STRESS ANALYSIS OF THE COIL SUPPORT STRUCTURE

	Gas-cooled HTS	CICC LTS	Indirect-cooled LTS
Von Mises stress (MPa)	683	691	720
Amount of deformation (mm)	23.3	23.6	24.9
Axial strain in HC (%)	0.183	0.188	0.207
Shear strain in HC (MPa)	34	31	31

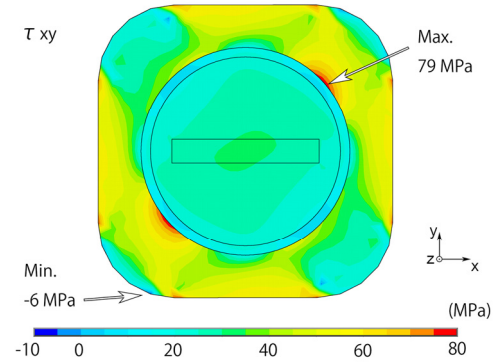


Fig. 5. In-plane shear stress distribution of the superconductor unit at the location of maximum in-plane shear stress in the HC for the gas-cooled HTS.

analysis. We focused on the region of maximum in-plane stress (Fig. 4), since shear stress on the insulator is one of the critical issues for the superconducting magnet system. Fig. 5 shows the in-plane shear strain distribution of the cross-section of the conductor, for the gas-cooled HTS. The main shear stress occurred at the outer stainless steel jacket. The shear stress in the YBCO tape stack region was equal to or less than the shear stress in the whole-structure analysis.

The shear strength of an insulator using fiber reinforced plastic (FRP) depends on the applied compressive load. Fig. 6 shows a normal stress (in the direction of lamination) and an in-plane shear stress distribution, expressed by the cylindrical coordinates shown. Although the precise materials and composition of the insulator has not yet been decided, two estimations were conducted. One used the “LHD criterion” adopted for the assessment of the inner VFC of the LHD [17]. The other used the “ITER criterion,” referencing the estimation method for the insulator of the ITER TF coil [12]. The fracture criterion curve of the insulator in the Mohr–Coulomb theory, and the strength of the LHD insulator, is given by

$$(\sigma_n / \sigma_{n0}) + (\tau / \tau_0)^2 = 1 \quad (1)$$

$\sigma_{n0} = 38 \text{ MPa}, \tau_0 = 27 \text{ MPa at } 77 \text{ K},$

where,  $\sigma_n$  and  $\tau$ , are the normal stress in the lamination direction and the in-plane shear stress of the lamination cross-section, and  $\sigma_{n0}$  and  $\tau_0$  are the tensile and shear strengths under uni-axial loading, determined experimentally. The fracture criterion curve of the “ITER criterion” and the strength are expressed as

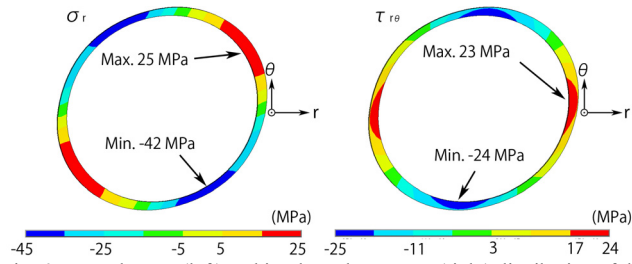


Fig. 6. Normal stress (left) and in-plane shear stress (right) distribution of the insulator in the gas-cooled HTS.

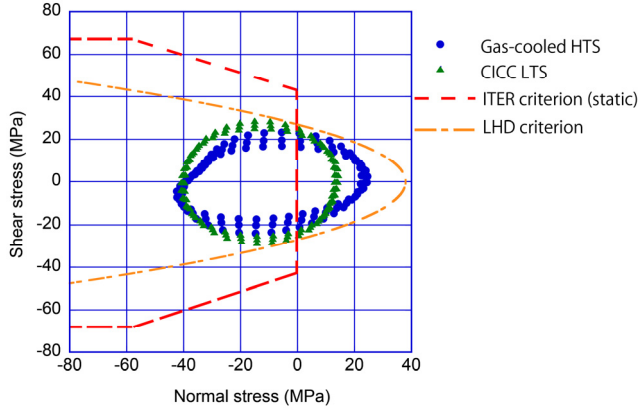


Fig. 7. Correlation between the shear stress and the normal stress in the insulator obtained from the localization analyses for the gas-cooled HTS type and the CICC LTS-type superconductor. Calculated strength criteria according to eqs. (1) and (2) are also indicated.

$$\begin{aligned} \tau &= \tau_0 / 2 + 0.45 \times \sigma_n, \quad \text{when } -58 < \sigma_n \leq 0 \text{ MPa} \\ \tau &= 68.6 \text{ MPa}, \quad \text{when } \sigma_n \leq -58 \text{ MPa}. \\ \tau_0 &= 85 \text{ MPa at } 4 \text{ K}. \end{aligned} \quad (2)$$

The tensile stress could not be applied to the insulator, because the shear stress under compressive load in the lamination direction is only available in the ITER criterion. The shear strength in (2) was for the static case, and was taken from the database for the ITER TF coil. Fig. 7 shows the scatter plot of the shear stress and the normal stress on the insulator, in the gas-cooled HTS and the CICC LTS superconductors. The allowable limits under the LHD and ITER criteria are also shown. The shear stress was within both criteria, when the normal stress had a negative value, i.e. under compression. However, when both tensile and shear stress were applied simultaneously, the results fell outside the ITER criterion. Further experimental evaluation is needed for selection of the insulator.

### III. FEASIBILITY STUDY OF SEGMENTED WINDING

The construction of the helical fusion reactor is an important issue, and segmented fabrication has been proposed for the HC. A simple stacking HTS conductor and its mechanical lap joint have been developed and a sample conductor successfully achieved 100 kA current [6], [7]. In segmented fabrication, the length of the segment and the number of joints within the section are important, both from the perspective of fabrication and of their thermal properties.

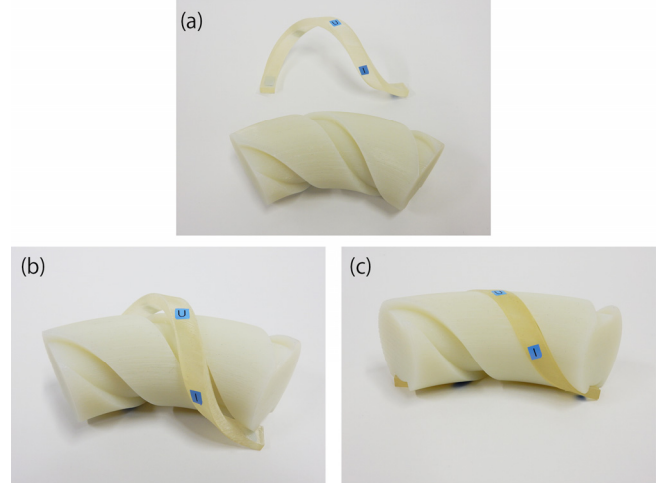


Fig. 8. Photo images of the 1/20-scale 3D printer models used for the feasibility study of segmented fabrication of the helical coil (original cross-section: 1860 mm width  $\times$  930 mm height). The groove in the coil casing is 1.075 times larger than the coil winding pack (a). One pitch of the helical coil (starting from the bottom, through the inner, upper, outer parts, and ending at the bottom (b)) can be inserted into the helical coil casing without giving additional force (c).

Feasibility studies of winding were conducted using the 3D CAD system and 3D printing. The 3D printing model identified the gap width required to insert the conductor segment into the coil casing. As the result of trial and error approach using the 3D printing, it was found that a maximum one helical pitch of coil segment could be inserted into the coil casing without deformation, if the groove of the casing was more than 1.075 times the coil winding pack. This is shown in Fig. 8. In the actual manufacturing, the joint winding will be performed for every single superconductor. It is considered to install segments of conductors, not segments of the whole winding pack, and thus, the necessary gap will be 62 mm + 4.65 mm. There is an enough gap for inserting a conductor except the last turn of each winding layer. The necessary gap of 4.65 mm is for the conductor at the last turn. After one conductor at any turn is inserted to its appropriate position, the conductor can be pulled up to free space with relatively small bending force. For example, the cantilever beam with length of 7.5 m (quarter length of one pitch of helical coil winding), 62 mm  $\times$  62 mm square shape, and longitudinal Young's modulus of 114 GPa, can be bent 500 mm with force of 500 N at the free edge of the beam. Joint work will be established in this free space.

### IV. CONCLUSIONS

The LHD-type helical reactor FFHR-d1 is under fundamental design phase. There are several candidate for superconducting magnet system. A CICC LTS-type is the basic option for FFHR-d1 since it is a mature technology for a large scale magnet like the ITER. However, a length of a cooling path can be limited for a huge scale magnet beyond ITER. An indirect-cooled LTS-type solves this problem but careful design study is needed, such as a thermal stability and a contact control between a cooling panel and a superconductor. For both LTS-type, there are another issues

that the continuous winding and a vacuum pressure impregnation process after winding are needed. The gas-cooled HTS-type has a potential to solve issues in the LTS-type. The selection of conductor type will be made after research and development activities are completed for each conductor type together with the design progress.

Multi-scale structural analysis is useful in assessing the alternative cooling schemes and superconductors at the development phase of design. The results of the multi-scale analysis for the magnet system of the helical reactor suggest that the longitudinal rigidity of the superconductor is the major determinant of stress in the coil support structure. The mechanical behavior of the insulator was also investigated and compared with the fracture criteria.

Segmented fabrication with one pitch of helical coil winding, using 3D printing, appears to be possible, based on the feasibility study.

#### REFERENCES

- [1] A. Sagara, et al., "Design activities on helical DEMO reactor FFHR-d1," *Fusion Eng. Des.*, vol. 87, issues 5–6, pp. 594–602, Aug. 2012.
- [2] A. Sagara et al., "Helical reactor design FFHR-d1 and c1 for steady-state DEMO," *Fusion Eng. Des.*, vol. 89, issues 9–10, pp. 2114–2120, Oct. 2014.
- [3] S. Imagawa, et al., "Concept of magnet system for LHD-type reactor," *Nucl. Fusion* 49 075017 (8pp), 2009.
- [4] K. Takahata, H. Tamura, T. Mito, S. Imagawa, and A. Sagara, "Development of an indirectly cooled superconductor for LHD fusion reactor FFHR," *Plasma and Fusion Research* 9 3405034 (4pp), 2014.
- [5] K. Takahata, H. Tamura, T. Mito, S. Imagawa, and A. Sagara, "A cooling concept for indirectly cooled superconducting magnet for the fusion reactor FFHR," *Plasma and Fusion Research* 10 3405011 (4pp), 2015.
- [6] N. Yanagi, et al., "Design and development of high-temperature superconducting magnet system with joint-winding for the helical fusion reactor," *Nucl. Fusion* 55 053021 (7pp), 2015.
- [7] S. Ito, H. Oguro, H. Tamura, N. Yanagi, and H. Hashizume, "Fundamental investigation on tensile characteristics of a mechanical lap joint of REBCO tapes," *IEEE Trans. Appl. Supercond.*, Vol. 25, no. 3, Jun. 2015, Art. ID 4201205.
- [8] K. Terada, J. Kato, N. Hirayama, T. Inugai, and K. Yamamoto, "A method of two-scale analysis with micro-macro decoupling scheme: application to hyperelastic composite materials," *Comput. Mech.* Vol. 52, Issue 5, pp. 1199–1219, Nov. 2013.
- [9] J.W. Ekin, *Experimental Techniques for Low-Temperature Measurements: Cryostat Design, Material Properties, and Superconductor Critical-Current Testing*. Boulder, CO, USA: Oxford Univ. Press, 2006.
- [10] Y. Iwasa, *Case Studies in Superconducting Magnets: Design and Operational Issues*, 2nd ed. New York, NY, USA: Springer-Verlag, 2009.
- [11] N. Mitchell, "Finite element simulations of elasto-plastic processes in Nb3Sn strands," *Cryogenics* Vol. 45, Issue 7, pp. 501–515, Jul. 2005.
- [12] ITER Structural Design Criteria for Magnet Components (SDC-MC), N11 FDR 5001-07-05 R 0.1, Naka, Japan, 2001.
- [13] H. Tamura, et al., "Novel divertor design to mitigate neutron irradiation in the helical reactor FFHR-d1," *Fusion Eng. Des.*, vol. 88–89, pp. 1629–1633, Oct. 2015.
- [14] H. Tamura, et al., "Design of structural components for the helical reactor FFHR-d1A," *Fusion Eng. Des.*, vol. 89, issues. 9–10, pp. 2336–2340, Oct. 2014.
- [15] Y. Chida, et al., "Validation of welding technology for ITER TF coil structure," *Fusion Eng. Des.*, vol. 86, issue 12, pp. 2900–2903, Dec. 2011.
- [16] H. Song et al., "2G HTS coil technology development at SuperPower," *IEEE Trans. Appl. Supercond.* Vol. 23, no. 3, Jun. 2013, Art. ID 4600806.
- [17] K. Kitamura *et al.*, "Cryogenic shear fracture tests of interlaminar organic insulation for a forced-flow superconducting coil," *IEEE Trans. Magnetics*, vol. 30, no. 4, pp. 1879–1882, Jul. 1994.